Doctor of Philosophy

Evaluation of Vascular Permeability in Alzheimer's Disease using Dynamic Susceptibility Contrast Magnetic Resonance Imaging (DSC-MRI)

The Graduate School

Of the University of Ulsan

Department of Medicine

Hana Kim

Evaluation of Vascular Permeability in Alzheimer's Disease using Dynamic Susceptibility Contrast Magnetic Resonance Imaging (DSC-MRI)

Supervisor : Jae-Hong Lee

A Dissertation

Submitted to

The Graduate School of the University of Ulsan

In partial Fulfillment of the Requirements

For the Degree of

Doctor of Philosophy

by

Hana, Kim

Department of Medicine

Ulsan, Korea

August, 2019

Evaluation of vascular permeability in Alzheimer's disease using Dynamic susceptibility contrast magnetic resonance imaging (DSC-MRI)

This certifies that the dissertation of Hana Kim is approved.

Committee Vice-chair Dr. Dong-Wha Kang

Committee Member Dr. Jae-Hong Lee

Committee Member Dr. Geon-Ho Jahng

Committee Member Dr. Eun-Jae Lee

Committee Member Dr. Yeon-Jung Kim

Department of Medicine

Ulsan, Korea

August, 2019

Abstract

Background

Although amyloid plaques and neurofibrillary tangles have been considered main pathology of Alzheimer's disease (AD), therapeutic trials targeting these molecules have not been successful. Recently, vascular contributions to Alzheimer's disease (AD) are increasingly reported, suggesting that the integrity of blood-brain barrier (BBB) may play a critical role in disease mechanism. Detecting subtle BBB leakage in AD have been challenging, but recently several studies showed evaluation of BBB disruption with perfusion MRI. Dynamic susceptibility contrast (DSC) perfusion imaging is applied to evaluate cerebral blood volume in tumors and strokes in the brain, but has not applied to detect the disintegrity of BBB, especially in AD. Therefore, this study aimed to investigate the preclinical and clinical applicabilities of DSC-MRI to detect BBB disruption in AD-model mouse and AD.

Methods

For the preclinical study, DSC-MRI was obtained in two strains of Alzheimer transgenic mice (4 to 20 months old), which were 13 5xFAD mice (8 with transgenic mice, 5 with wild-

type mice) and 8 Tg2576 mice (4 with transgenic, 5 with wild-type) and their age-matched wild-type mice using Gadolinium contrast injection. Cerebral blood volume (CBV), cerebral blood flow (CBF), extraction fraction and leakage parameters were calculated and analyzed. Group comparison with region-of-interest (ROI) and voxel-based analysis were performed to compare the difference of permeability index in two groups. After MR imaging, mice were sacrificed and immunohistology of their brains were evaluated to compare the extent of amyloid plaques and endothelium structure. For the clinical study, DSC-MRI was also obtained in 10 AD patients and 13 age-matched controls for the pilot study. Perfusion indices were calculated to compare between the two groups with voxel-based and ROI-based analyses.

Results

For the animal study, the ROI-based quantitative measurements of DSC map showed higher permeability indices in the hippocampus of 5xFAD mice compared with those of WT mice. VBM analysis of leakage maps revealed significant differences in left frontal cortex and dorsal hippocampus between two groups (p=0.01). Temporal increase of leakage was more prominent in AD group than in control group (p=0.042). For the clinical study, in AD group,

leakage value increased at right putamen (p= 0.012), thalamus (p= 0.035) and extraction fraction also increased at left corpus callosum (p< 0.001), right cingulate gyrus (p= 0.004) and parahippocampal gyrus (p= 0.016) compared with the control group.

Conclusions

DSC-MRI revealed BBB disruption in AD mouse models, and most frequently affected locations were left frontal cortex and hippocampus. Human pilot study also showed higher permeability index in several gray matter and white matter regions of AD patients, indicating that DSC-MRI also detects BBB disruptions in a human study. Our findings suggest that abnormalities in DSC-MRI may be a feasible biomarker to detect impaired BBB function in AD patients, which should be explored in further clinical studies.

Contents

List of Tables and Figures

Abbreviations

Aβ amyloid beta

AD Alzheimer's disease AD

BBB blood-brain barrier

CA contrast agent

CBV cerebral blood volume

CNS central nervous system

DCE dynamic contrast-enhanced

DSC dynamic susceptibility contrast

MCI mild cognitive impairment

VBM voxel-based morphometry

I. Introduction

I.1. Blood-brain barrier (BBB) in Alzheimer's disease (AD)

Alzheimer's disease (AD) is a neurodegenerative disease characterized by progressive cognitive impairment including memory deficit. Pathophysiology for AD is represented by intracellular neurofibrillary tangles of hyper-phosphorylated tau and amyloid-β (Aβ) peptide. However, a large number of therapeutic trials targeting these molecules have been failed. Recently, evidence of vascular contributions to AD pathophysiology is increasingly reported[1-3] suggesting that the integrity of blood-brain barrier (BBB) may play a critical role in the disease mechanism.

The blood-brain barrier (BBB) maintains the stability of central nervous system (CNS) by limiting the entry of toxic metabolites – plasma-derived components, RBCs, leukocytes, and pathogens.[4] Interest in the role of the BBB surged over the past decade because a large number of neurological diseases – small vessel disease, dementia – are linked to BBB disruption. Accordingly, various methods to assess BBB disruption in AD have been suggested in previous studies.[2 5]; Histologic results and the albumin ratio measurement showed BBB degradation in

AD.[2] Other researchers reported BBB disruption in AD by post-mortem studies with accumulation of blood-derived proteins in hippocampus and cortex.[6-9] Several brain imaging studies found microbleeds in the hippocampus of AD.[10] However, imaging technique of region-specific BBB permeability has been challenging since the leakage starts subtle and the signal to noise ratio is low in neurodegenerative disorders.[11]

I.2. MRI studies to investigate BBB breakdown in AD

Cerebrovascular Imaging is represented by perfusion MRI including dynamic contrast enhanced (DCE) MRI, arterial spin labeling (ASL) MRI, and dynamic susceptibility contrast (DSC) MRI. For ASL-MRI, a non-equilibrium state is generated to tag inflowing spins at a level proximal to the imaging slab. Images are recorded following a transit delay to allow these tagged spins to enter the imaging and exchange with tissue. Quantitative cerebral blood flow (CBF) values can be obtained from ASL images. Imaging of the BBB with DCE-MRI has been widely used in brain tumors or metastases, head trauma and stroke models. However, ASL-MRI has not been routinely used in clinical study because of a low signal-to-noise ratio

compared to DSC and DCE method. DCE-MRI is acquired during intravenous injection of contrast agent (CA), usually Gadolinium-based. With DCE-MRI, CA volume transfer constant (K^{trans}), which reflects vascular permeability and perfusion, is computed by kinetic analysis of altered T1 relaxation time.[12] DCE-MRI is a standard imaging method to evaluate BBB breakdown and has been widely used in brain tumors or metastases, head trauma and stroke models. However, the scan time of DCE-MRI is usually too long to obtain a good permeability image in case of degenerative disease including AD because of slow leakage of CA[13 14]; therefore, it is hard to apply in clinical practice of AD patients.

In DSC-MRI, T_2*-weighted images are acquired serially, and regional changes of MRI signal intensity are measured as the CA traverses the cerebral vasculature. This information is then converted into contrast-time curves and hemodynamic parameters, to calculate mean transit time (MTT), cerebral blood volume (CBV) and CBF. The intravascular indicator dilution theory has been used in the process and the theory assumes that the CA remains intravascular during its passage. Modeling of the leakage contribution to the image signal intensity change has been used to obtain information on the vascular transfer constant, BBB permeability.[15]

DSC-MRI has been used only in the brain tumors or cerebral ischemia for the measurements of cerebral perfusion. DSC-MRI has an advantage of relatively short acquisition time compared to DCE-MRI, and therefore it should be optimal to apply in AD patients.

a) In animal experiments

As quantitative CBF values can be obtained from ASL images, ASL method was applied to overexpressing APP mouse strains in several studies.[16-18] Reduced CBF was observed in cortex, while perfusion was normal in subcortical area. DSC-MRI was also used for measuring CBF in animal model. Though CA injection is needed for the DSC method, scan time is faster and signal-to-noise is higher than ASL images. For DCE method, it has been used to predict the hemorrhage occurrence in ischemic stroke.[19] BBB disruption was hardly found with mouse DCE-MRI in earlier studies because the leakage is subtle and diffuse in neurodegenerative disease while stroke or tumor cases present large and focal leakage. A recent study however, reported the difference of permeability index in late stage of the disease

was detected with DCE-MRI.[20] DSC-MRI provides highly sensitive perfusion information and can be used to estimate the exogenous tracer concentration. It can also be used to extract information regarding cerebral perfusion on drug tracer models

b) In human brain studies

DCE-MRI studies of BBB permeability in AD or mild cognitive impairment (MCI) showed controversial results in earlier studies.[21 22] However, several studies reported that BBB leakage occurs in early stage of AD with DCE-MRI.[11 23 24] A study with MCI patients showed altered BBB integrity in the hippocampus, while the other study suggested that BBB impairment appears widespread than localized to a single tissue in early AD patients. According to recent report, permeability index obtained from DCE-MRI was showed correlation with cognition and ROI quantification of hippocampus was higher in patients with AD than MCI.[13]

1.3 Dynamic Susceptibility Contrast (DSC) MRI to Evaluate BBB Breakdown

Since one of the model assumptions is intact BBB, CA extravasation is a confounding factor in the kinetic analysis of DSC-MRI, leading to underestimation of blood volume. Therefore correction for CA leakage effect is essential with techniques developed by Weisskoff et al[25 26] and Boxerman et al.[27] In the process of the correction, leakage parameter reflecting the degree of CA extravasation termed "K_2" can be extracted. Leakage effect of tissue is postulated with DSC-MRI and its clinical eligibility to brain tumors has been suggested in a few studies.[28 29] However, there has been no study applying DSC-MRI to AD patients for evaluation of BBB disruption.

I.4. Purpose

The use of DCE-MRI for the evaluation of vascular permeability is a well-established method, however, needs a longer scan time to detect subtle disruption in a neurodegenerative disease. It is a matter in clinical settings, as demented patients hardly stand even conventional scan time without motion. Accordingly clinical feasibility of the technique is questioned and for this reason DCE-MRI is not used routinely in the clinic for diagnosis[30] forming its position as

a research tool. BBB disruption is increasingly reported to start in the early stage of AD, therefore clinically feasible imaging tool is needed. Though there was an attempt to postulate the leakage parameters reflecting vascular permeability in DSC-MRI using correction techniques as mentioned above,[31] studies investigating vascular permeability in AD with DSC-MRI is absent. Therefore, the objectives of this thesis were to validate the feasibility of BBB breakdown in AD-model mouse using DSC-MRI, and to correlate the imaging to the pathology. Serial follow up of MRI was also performed to compare the young-aged and old-aged mice and show the temporal change. By extension, a human pilot study was conducted with DSC-MRI in patients with Alzheimer's disease and age-matched controls.

II. Materials and Methods

II.1 Animals

II.1.1. Alzheimer transgenic mouse model

5xFAD mice overexpress the K670N/M671L (Swedish), I716V (Florida), and V717I (London) mutations in human APP (695), as well as M146L and L286V mutations in human PS1. Hemizygous transgenic 5xFAD (TG) and wild-type B6SJL/J (WT) mice were obtained from the Jackson Laboratory. Experiments were also performed in Tg2576 mice harboring the Swedish mutation of APP. Overall study design is shown in Figure 1. Cross-sectional study with Tg2576 young- and old-aged mice and follow up study with 5xFAD mice was designed in this study. To minimize confounding effects of background heterogeneity and genetic modifiers, experiments were performed in age-matched littermates, female mice (Table 1A, 1B). All procedures were approved by the Institutional Animal Care and Use Committee of Asan Medical Center.

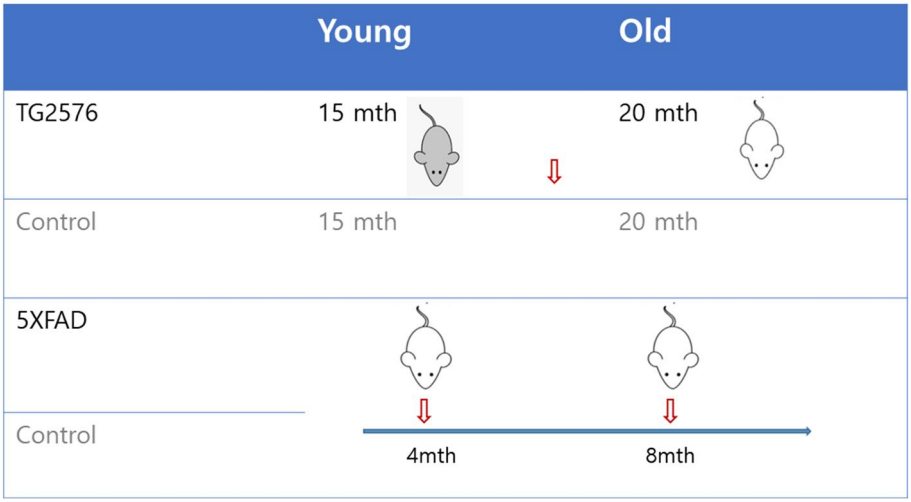

Figure 1. Study design of animal experiments

Tg2576 model mice aged 15 months and 20 months with age-matched controls conducted DSC-MRI for cross-sectional study. 5xFAD mice and age-matched controls conducted DSC-MRI in early stage (4months) and followed up at the age of 8 months. mth, months

A

Mouse model	Age (months)	Tg (n)	NTg (n)
Tg2576	15	3	2
	18	2	3
	20	4	4
5xFAD	3	2	2
	4	3	2
	8	9	6

B

Mouse model	Interval (months)	Tg (n)	NTg (n)
Tg2576	2-5	4	4
5xFAD	4	3	2

Table 1. Number of transgenic and control mice

A, Number of MRI scans of 5xFAD and Tg2576 mice; B, Number of follow up scans. Tg, transgenic mice; NTg, non-transgenic (control) mice

II.1.2. MRI acquisitions

For MRI examinations, the mice were positioned on a mouse cradle and anesthetized using isoflurane (1.0%-1.5%). During MRI examination, respiration rate was monitored, and body temperature was maintained to be at 37°C using warm airflow. MRI was performed on a 7.0 T Bruker PharmaScan 70/16 MRI system (Bruker BioSpin, Ettlingen, Germany) with Paravision 6.0.1 software in a configuration of a 72 mm transmit volume coil and a mouse brain surface receiver coil. Prior to intravenous CA injection, T2-weighted images (T2WIs) were obtained using the fast-spin echo sequence. Brain permeability was assessed after injection of Gadolinium (Gadovist®, 0.2 mmol/kg) using DSC-MRI technique. The MRI protocol was composed of T2-WIs, T1 maps, and DSC-MRI. The parameters for each sequence are shown in Table 2.

	T2-WI	T1 map	DSC-MRI
TR (ms)	4000	656/900/1500/ 2500/40000/7000	1000
TE (ms)	33	12.15	16
Flip angle (°)	-	-	30
Averages	2	1	2
FOV (mm)	18 x 18	18 x 18	18 x 18
Acquired resolution (μm)	141	281	188
Rare factor	8	4	-
Slice number	18	18	18
Slice thickness (mm)	0.5	0.5	0.5
Duration (min:sec)	2:08	8:49	5:00

Table 2. Parameters for each MRI sequences (animal)

II.1.3. Data processing and Image analysis

NordicICE was used to obtain perfusion indices, including CBV, CBF, MTT, Leakage and Extraction maps. Vascular permeability with DSC-MRI was mapped using the previously suggested methodology.[31] Parameter maps were registered to mouse atlas with Jip-Align. Methodology for measuring vascular permeability with DSC-MRI was used. Then, K_2 is extracted from the equation below with the method proposed by Weisskoff et al.[25]

$$\Delta\widetilde{R_2^*}(t) \approx K_1 \times \overline{\Delta R_2^*(t)} - K_2 \int_0^t \overline{\Delta R_2^*(t)dt}$$

$\overline{\Delta R_2{}^*}$ is the average of $\Delta R_2{}^*$ from a mask of non-enhancing of brain voxels and $\Delta\widetilde{R_2{}^*}$ is the leakage affected estimate of $\Delta R_2{}^*$.

Voxel-based analyses and regions of interest (ROIs) analysis were performed to compare indices between transgenic and control groups. Figure 2 shows, 10 ROIs of the right and left hippocampus. ROIs were manually drawn by a person blinded to the genotype on each animal in accordance to the standard mouse brain atlas with Asan J (Asan Medical Center). ROIs were extracted from results of voxel-based analysis (left frontal cortex and dorsal hippocampus; shown in result table) and analyzed to compare permeability indices.

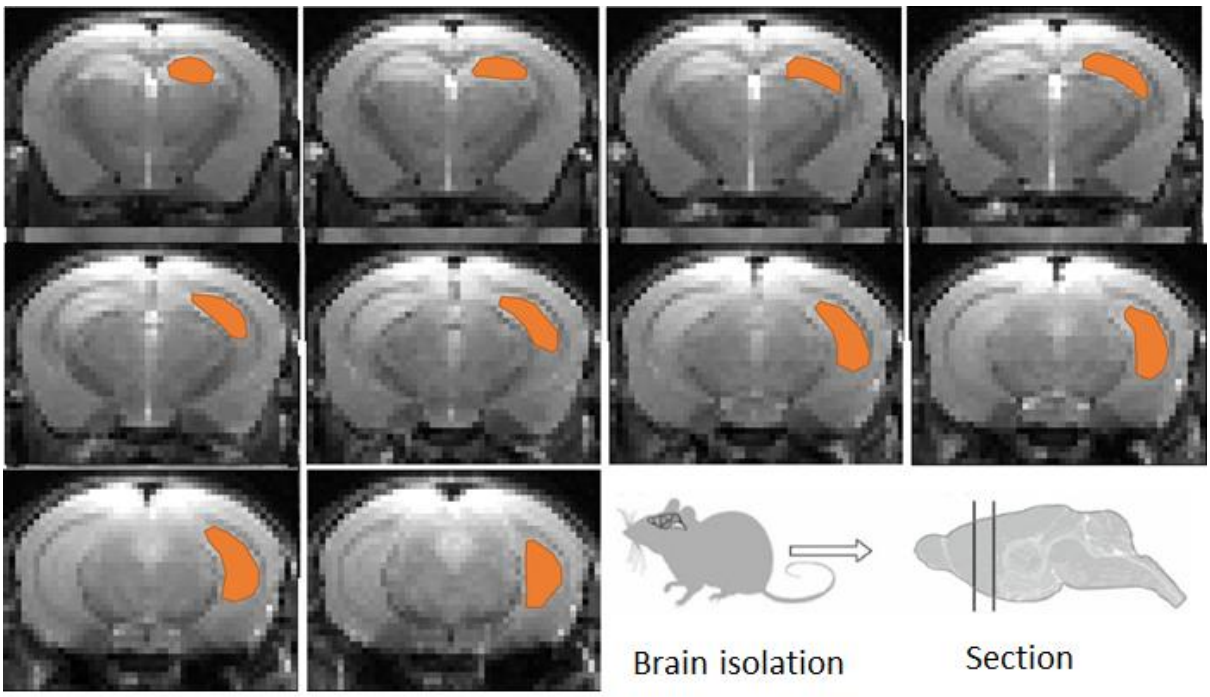

Figure 2. Examples of ROI (Left) in coronal images of mouse brain

ROI covering hippocampus was manually drawn on T2WI of mice. Ten ROI slices were averaged. The cartoons shown at the bottom were adapted from a preclinical study[12] ROI, Region of interest; T2WI, T2-weighted image

II.1.4. Histology

All animals were sacrificed after in vivo MRI experiments for immunohistological evaluation to investigate whether Aβ deposition driven by Alzheimer transgenic mice is associated with pericyte disruption. For immunostaining, sections were first rinsed in PBS 0.1 M and then in 30% hydrogen peroxide (H2O2). Then, they were pretreated with 0.2% octylphenol ethylene oxide condensate (Triton X-100™, Sigma-Aldrich®). After this pretreatment, they were incubated with an anti-amyloid primary antibody (6E10, dilution 1:2000) for 48 hours and then with a secondary antibody (anti-mouse, BA-9200, dilution 1:1000, Vector®) for 1 hour. Pericyte was visualized using PDGFβ (PDGFβ, dilution 1:1000).

II.2. Human Study

II.2.1. Subjects

Normal control and AD participants were recruited from memory clinic of Asan Medical Center (AMC). The DSC-MRI procedure was approved by AMC Institutional Review Board (IRB). Table 3 summarized information of 23 subjects including 10 AD patients and 13 age-matched controls with normal cognition. All participants underwent brain MRI and MMSE for screening, and neuropsychological full test was done for people with memory complains or abnormal results on screening. Two neurologists confirmed the diagnosis according to the criteria of the National Institute on Aging and the Alzheimer's Association for AD. Patients with other cause for dementia or vascular risk factors were excluded to minimize the confounders.

	Age (years)	Sex	Disease duration (months)	MMSE	Vascular risk factor		
					HTN	DM	HL
AD 1	73	F	12	21	Y	N	N
AD 2	75	M	14	20	N	N	N
AD 3	79	F	2	15	Y	N	N
AD 4	89	F	6	17	Y	N	N
AD 5	61	M	14	19	Y	N	N
AD 6	60	M	12	22	N	N	N
AD 7	70	M	-	19	N	N	N
AD 8	55	F	7	20	N	N	N
AD 9	61	F	16	7	N	N	N
AD 10	58	F	12	20	N	N	N
NC 1	69	M	-	29	N	N	N
NC 2	78	M	-	-	N	N	N
NC 3	80	F	-	21	N	N	N
NC 4	62	M	-	29	N	N	Y
NC 5	69	M	-	25	N	N	N
NC 6	77	F	-	25	Y	N	Y
NC 7	71	F	-	29	Y	N	Y
NC 8	77	F	-	26	N	N	Y
NC 9	63	M	-	29	N	N	N
NC 10	56	M	-	28	N	N	N
NC 11	66	F	-	23	Y	N	Y
NC 12	69	F	-	30	Y	N	Y
NC 13	72	F	-	30	Y	N	Y

Table 3. Demographics of human subjects

II.2.2. MRI acquisitions

To map BBB leakage, DSC protocol was implemented for 3T MRI (Philips). DSC-MRI was acquired before, during, and after intravenous bolus injection (4 ml/s) of 0.1 mmol/kg CA (Gadoterate meglumine; Dotarem®) followed by injection of 20 ml of saline at a rate of 4 ml/s. The parameters for each sequence are shown in Table 4. The scan time of DSC-MRI was 4:35 (minutes: seconds).

	3D T1	T2 WI	DSC
TR (ms)	6.5	3000	1800
TE (ms)	2.9	80	32
FOV (mm)	256 x 256	220	220 x 234
Slice thickness (mm)	1	5	5
Acquisition matrix	256 x 256	400 x 255	132 x 135
SENCE	2		3
Slice number	211	20	24
Number of excitation	1		1
Duration (min:sec)	6:11		4:35
Dynamic scan			150

Table 4. Parameters for MRI protocol (human)

II.2.3. Data processing and Imaging analysis

a) DSC Parameter Mapping

NordicICE was also used to obtain perfusion indices, estimating CBF, CBV, MTT, leakage map, and extraction map from the DSC-MRI raw data.[32 33)] The method is validated for a range of signal-to-noise levels typical for DSC-MRI acquisitions and has been shown to provide more robust perfusion estimates than non-parametric approaches.[32 33)] Accordingly, all maps were normalized by corresponding values for normal appearing white matter identified on T1 weighted images (T1WI). Representative images are shown in Figure 3.

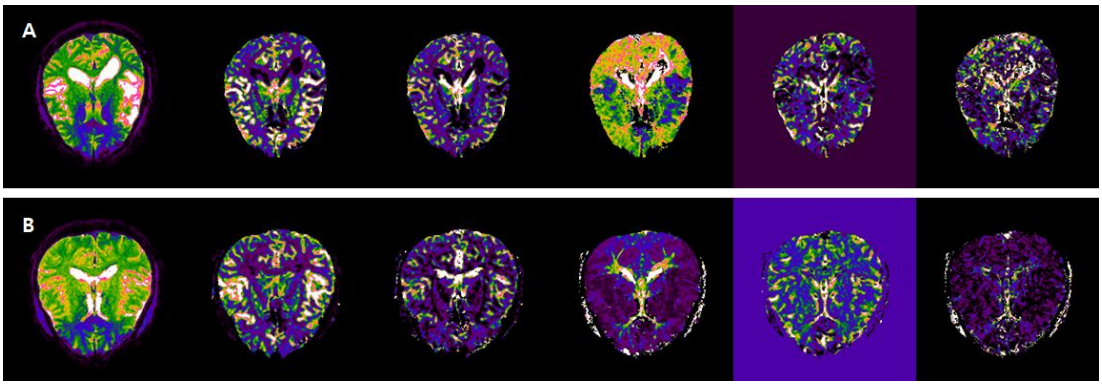

Figure 3. Representative images of DSC-MRI in human

Coronal view of DSC-MRI indices were obtained using nordicICE, including CBV, CBF, MTT, Leakage and Extraction maps. DSC first image – CBF – CBV – MTT – Leakage – Extraction fraction maps. **A** AD patients, **B** normal control

b) Post-Processing

To compare all perfusion maps between the two groups, all maps have to be spatially normalized into a standard brain template. Therefore, the three-dimensional (3D) T1WI and all perfusion indices were preprocessed using the framework described in previous report.[34] In this framework images are denoised using an estimated standard deviation of noise, bias field corrected, rigidly and non-rigidly registered to MNI space and skull stripped. With SPM12, firstly co-registration of 3D T1WI and DSC maps was done. Then, segmentation of 3D T1WI and normalization to the template was processed. Brain tissue is then classified into grey matter (GM), white matter (WM) and cerebrospinal fluid (CSF) using an artificial neural network classifier. Spatial normalization with these results was peformed, and finally smoothing for voxel-based statistical analyses was done.

II.3. Statistical Analysis

II.3.1. Animal experiment

a) Voxel-based analysis

To compare indices between the groups, voxel-based analyses were performed using the $p < 0.01$ and cluster-level $q < 0.01$ or 0.05 via AlphaSim (i.e., estimated number of significant voxels in a cluster from the statistics via Monte Carlo simulation; implemented in REST toolbox).

b) ROI-based analysis

For comparison of ROI results, repeated measures ANOVA was used. Statistical significance was accepted when the p value was < 0.05. Statistical analyses were performed using SPSS (SPSS Statistics for Windows, Version 17.0) and GraphPad Prism version 5 (GraphPad Software Inc., San Diego, CA, USA). Student t-test and Mann–Whitney U test for unpaired comparisons and the Wilcoxon test for paired comparisons were used.

II.3.2. Human study

a) Voxel-based analysis

For the group comparison of perfusion indices, voxel-based analyses were performed using $p < 0.005$. The uncorrected differences in all perfusion maps between the groups were first tested by using independent sample two-sided t test. Then, to evaluate the relationship between clinical parameters and perfusion indices, voxel-based correlation analysis was performed on $p < 0.001$ or $p < 0.005$. To investigate the association between BBB leakage and Mini-Mental State Exam (MMSE) score in two groups, corrected for age, linear regression analysis was used.

b) ROI-based analysis

I performed ROI analysis with atlas and voxel-based analyses. ROI placement was performed by Pick-Atlas with MATLAB, placed onto hippocampus, precuneus and thalamus. ROIs were selected based on previous studies about structures affected in early stage of Alzheimer's disease.[3 7 23)] A significant difference was inferred when a p value was less than 0.005. I also extracted MNI coordinates from results of voxel-based (left frontal cortex and dorsal hippocampus; shown in result table). Statistical analyses were performed using SPSS

(SPSS Statistics for Windows, Version 17.0) and GraphPad Prism version 5 (GraphPad Software Inc., San Diego, CA, USA). For the investigation of differences in the perfusion index values between the patients and control subjects, an independent-sample two-sided t test was used for each ROI.

III. Results

III.1. Animal experiment

T2*WI, CBF, CBV, Leakage and Extraction fraction maps were obtained from DSC-MRI and registered. Coronal view of T2*WI and DSC-MRI indices were displayed in Figure 4.

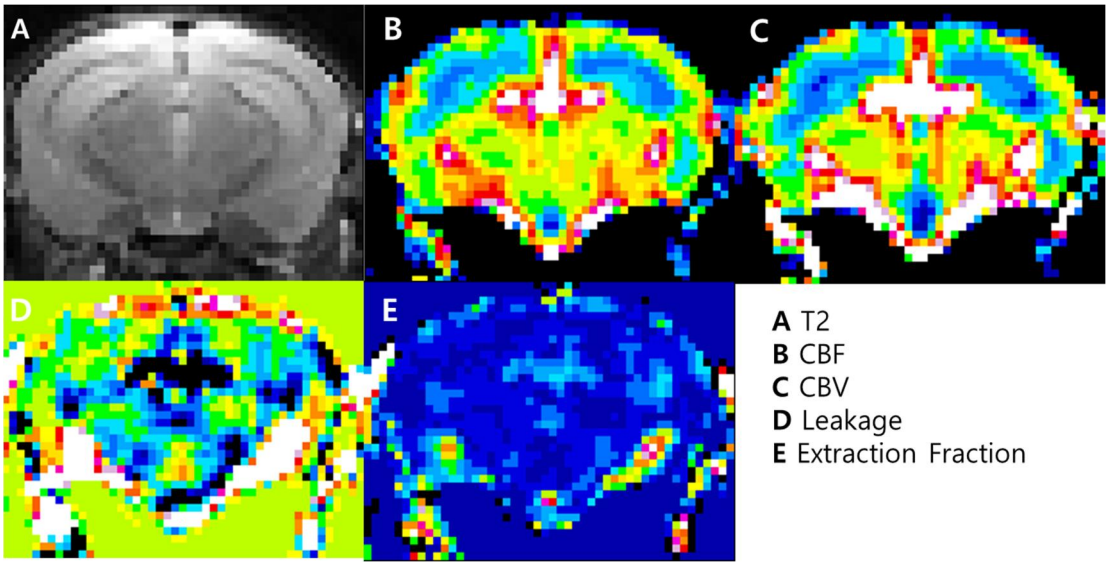

Figure 4. Representative images of DSC-MRI in mice

Coronal view of WT mouse. DSC-MRI parameters were measured using nordicICE, including CBV, CBF, MTT, Leakage and Extraction maps. **A** T2WI; **B** Cerebral blood flow (CBF); **C** Cerebral blood volume (CBV); **D** Leakage; **E** Extraction Fraction

III.1.1. Voxel Based Analysis

Figure 5 shows the results of voxel-based comparisons of leakage map between the 5xFAD transgenic and non-transgenic mice. There were clusters of significant (p<0.01) of leakage

indices in left frontal cortex and left dorsal hippocampus (Figure 5A). After alpha-cluster configuration, there left a cluster on frontal cortex (Figure 5B).

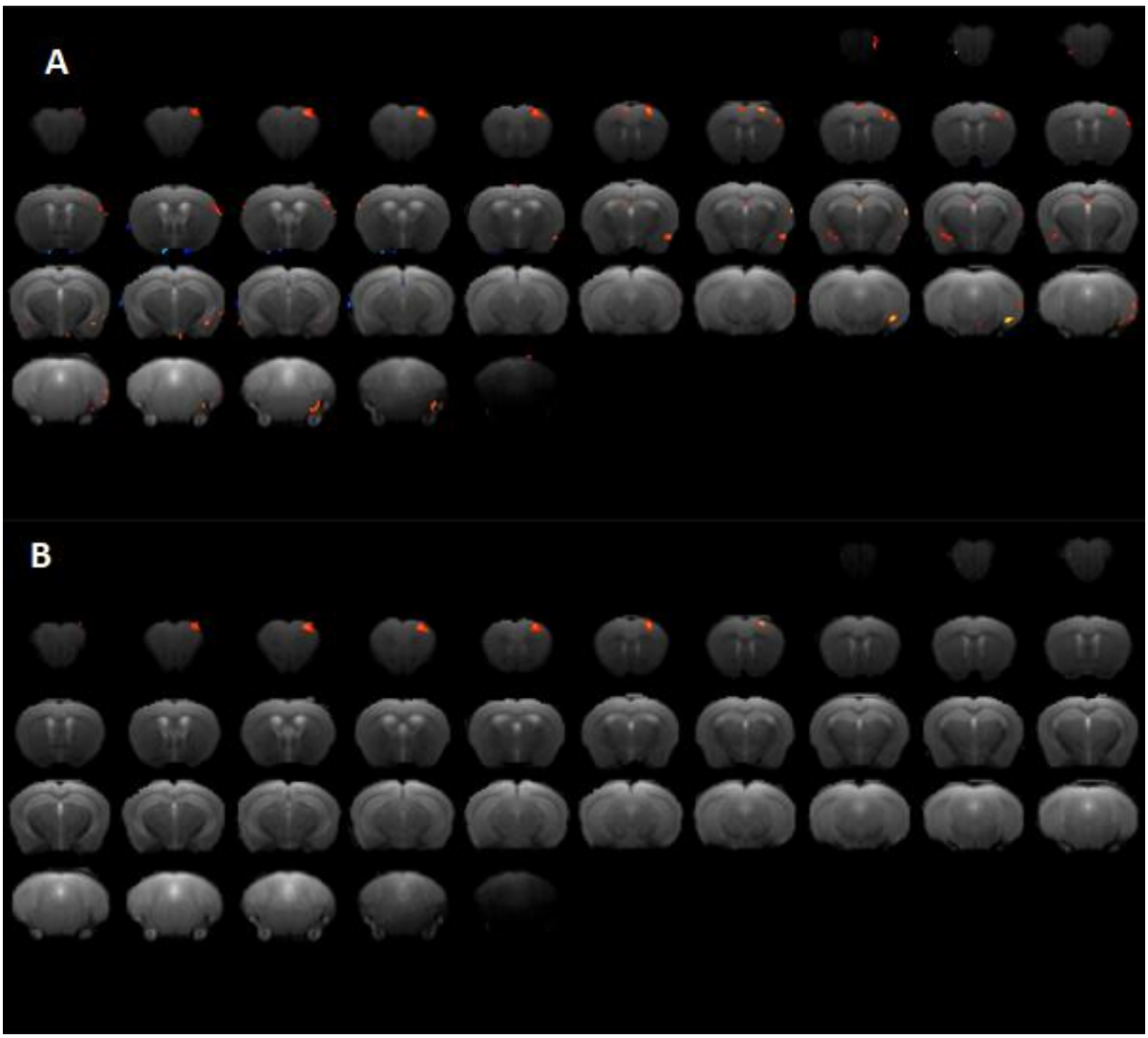

Figure 5. VBM analysis of leakage index between 5xFAD and non-transgenic mice

A, clusters of leakage indices before configuration; **B**, after configuration. There were clusters of significant (p<0.01) of leakage parameters in left frontal cortex and left dorsal hippocampus. After alpha-cluster configuration, there left a cluster on frontal cortex. Then, values from two clusters were extracted, which showed significant differences (left frontal cortex, p<0.005; dorsal hippocampus, p<0.001).

VBM analysis of Tg2576 and control mice showed few clusters in left hippocampus and subiculum, however no significant voxels existed after alpha-cluster configuration (Figure 6).

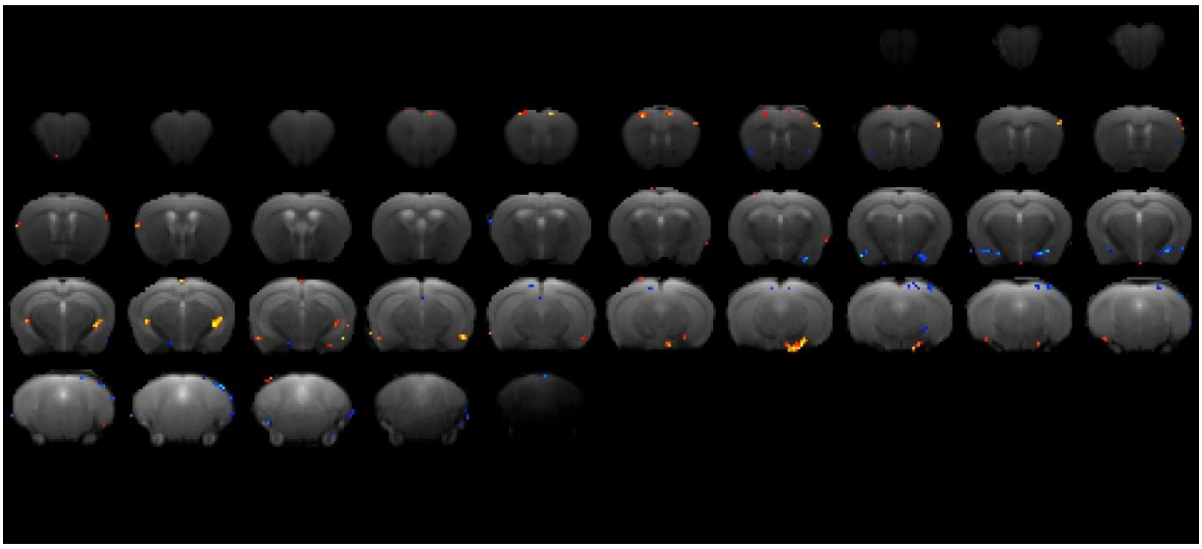

Figure 6. VBM analysis of leakage index between Tg2576 and non-transgenic mice

There were few clusters of significant (p<0.01) of leakage parameters in left hippocampus and subiculum.

III.1.2. ROI Analysis

For analyses of manually drawn ROI on hippocampus, in young mice (4 months), there was no difference in all indices of DSC-MRI (Figure 7) between two groups. In aged (8 months) mice, leakage indices of hippocampus were higher in transgenic mice without statistical significance (Right, p= 0.079; Left, p= 0.078) (Figure 8). The mean values of CBF, CBV and

extraction maps showed no difference between two groups. For temporal change of leakage maps, there was a difference between two groups (p= 0.042). Both 5xFAD transgenic and non-transgenic mice showed significant rise in leakage indices with increasing age, but the growth was larger in the transgenic group (Figure 9).

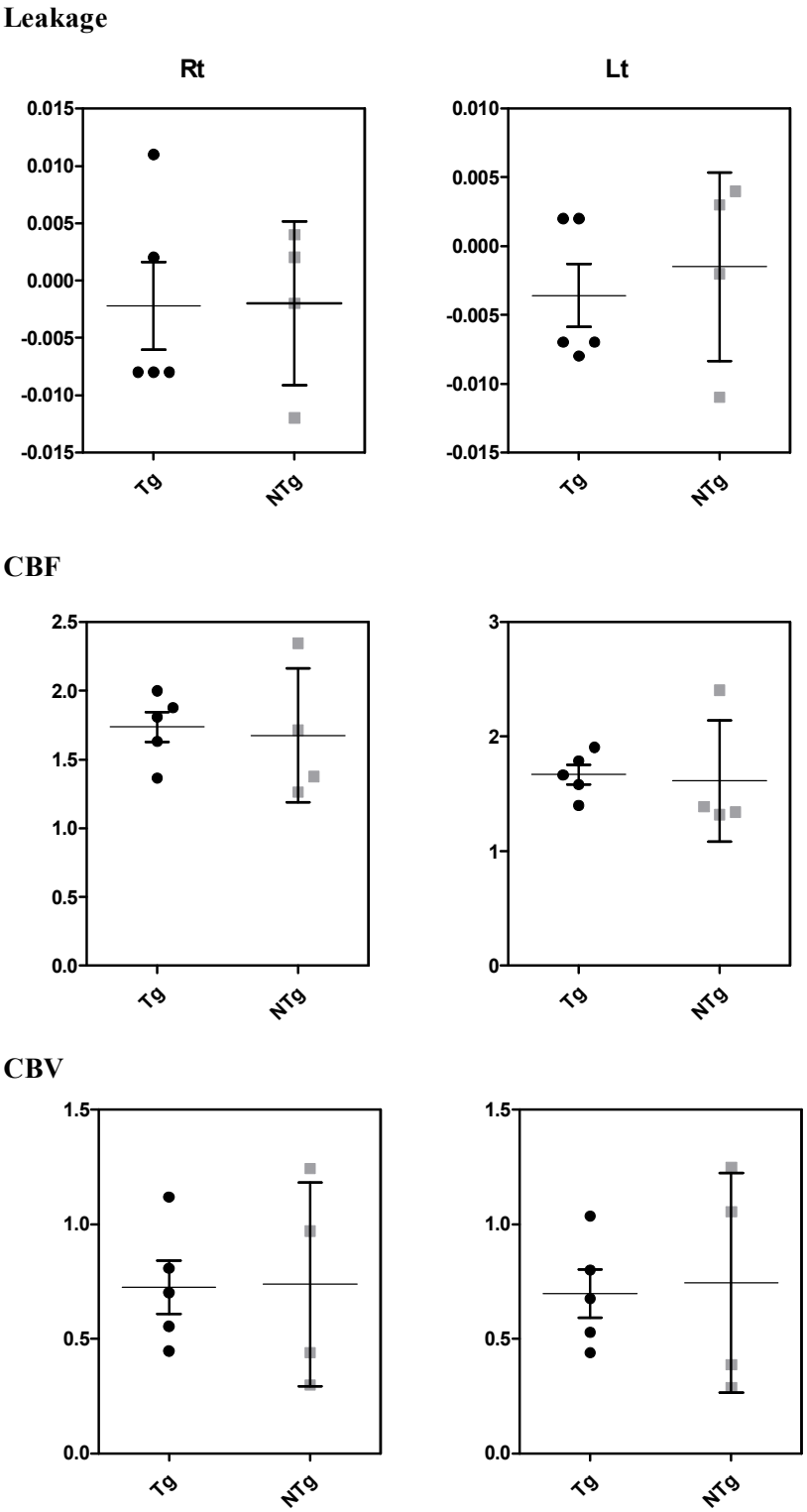

Figure 7. Scatter dot plots of CBV, CBF , Leakage parameters in young 5xFAD mice

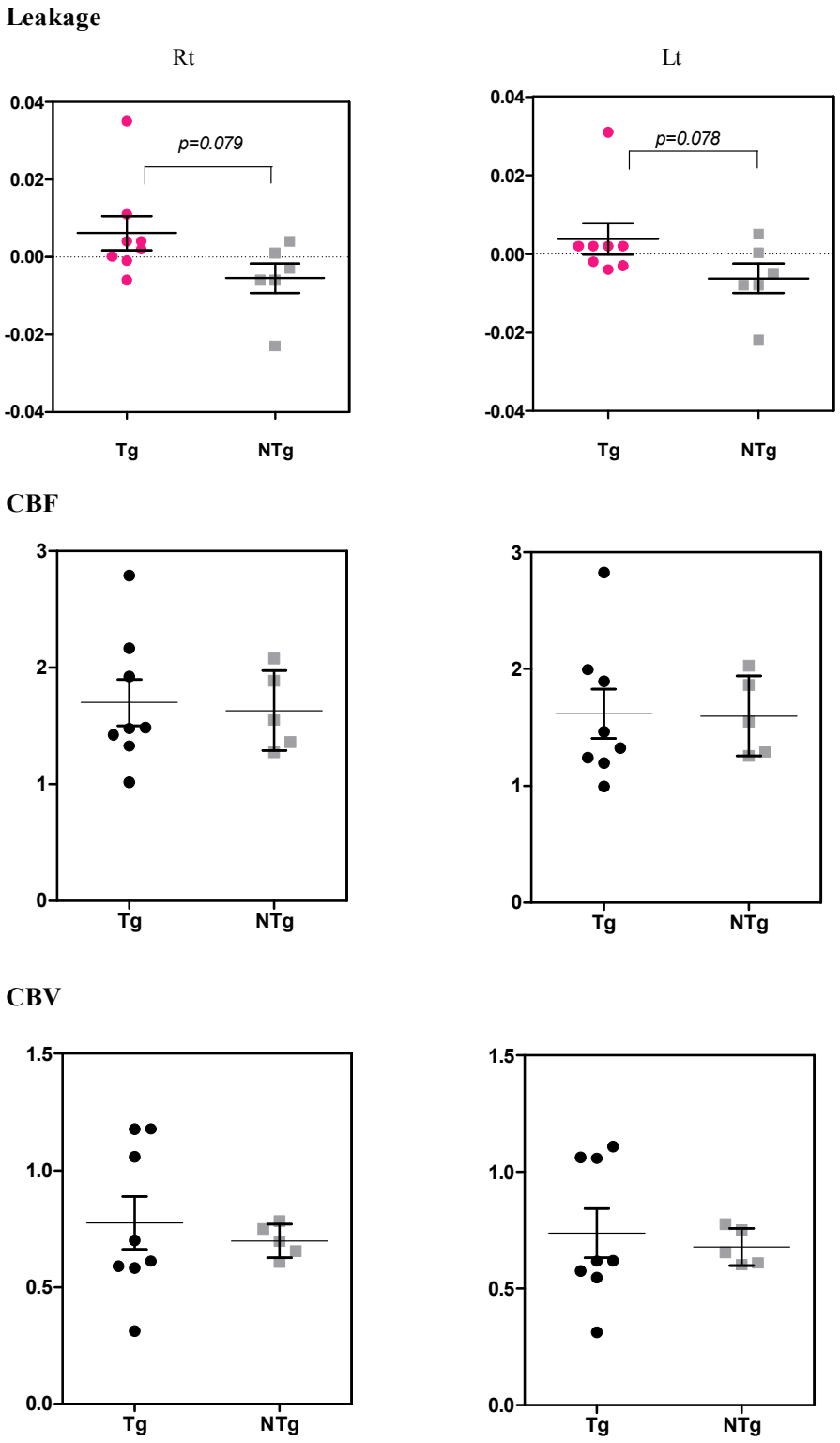

Figure 8. Scatter dot plots of CBV, CBF and Leakage parameters in old 5xFAD mice

In aged 5xFAD mice, higher BBB permeability was detected in hippocampus of transgenic mice compared with controls but the p-value was not sufficient (Rt, p= 0.079; Lt, p= 0.078). The mean values of CBF, CBV and Extraction maps showed no difference between two groups.

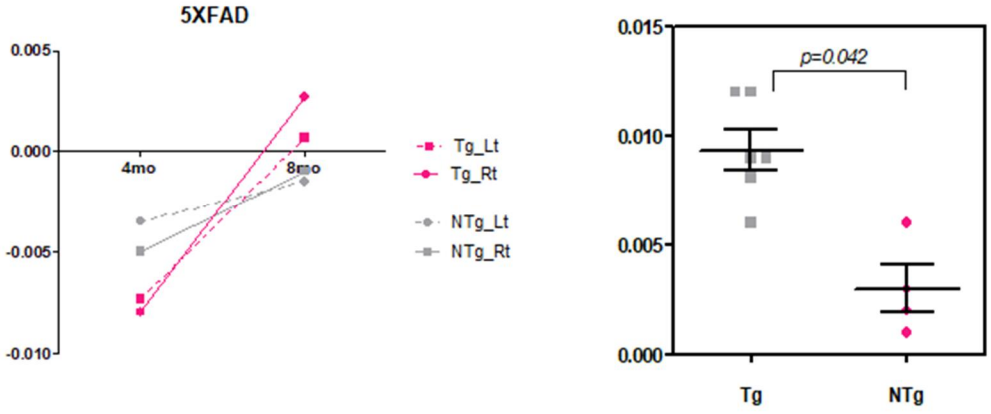

Figure 9. Temporal change of permeability index in 5xFAD mice (4mo-8mo)

Temporal change of leakage maps in two groups was statistically significant (*p*= 0.042).

For extracted values from two clusters of VBM analyses (Figure 5), higher values were shown in 5xFAD transgenic mice compared with controls with statistical significance (frontal cortex, p<0.005; dorsal hippocampus, p<0.001). Raw values of ROI were shown in Table 5.

	Lt frontal cortex	Lt dorsal hippocampus
Tg1	-1.28E-03	5.97E-03
Tg2	-1.47E-03	1.81E-03
Tg3	1.46E-02	8.85E-03
Tg4	-6.50E-03	4.17E-03
Tg5	-6.54E-03	4.88E-03
Tg6	1.82E-02	5.13E-03
NTg1	-1.11E-02	-5.71E-03
NTg2	-3.19E-02	-2.16E-02
NTg3	-2.24E-02	-1.89E-02
NTg4	-1.20E-02	-1.06E-02
NTg5	-3.70E-02	-1.06E-02
Cluster size	66	38
p-value	0.0042091	0.0001044

Table 5. Values of leakage obtained from two different areas from 5xFAD (Tg) and age-matched non-transgenic (NTg) mice

Extracted values from two clusters, left frontal cortex and dorsal hippocampus, were analyzed. Significant differences were shown between transgenic and control group.

When manually drawn ROIs were analyzed in Tg2576 mice and age-matched controls, there was no difference between two groups in all maps including leakage, extraction fraction, CBF and CBV maps. Temporal change of leakage parameters also showed a negative result (Figure 10).

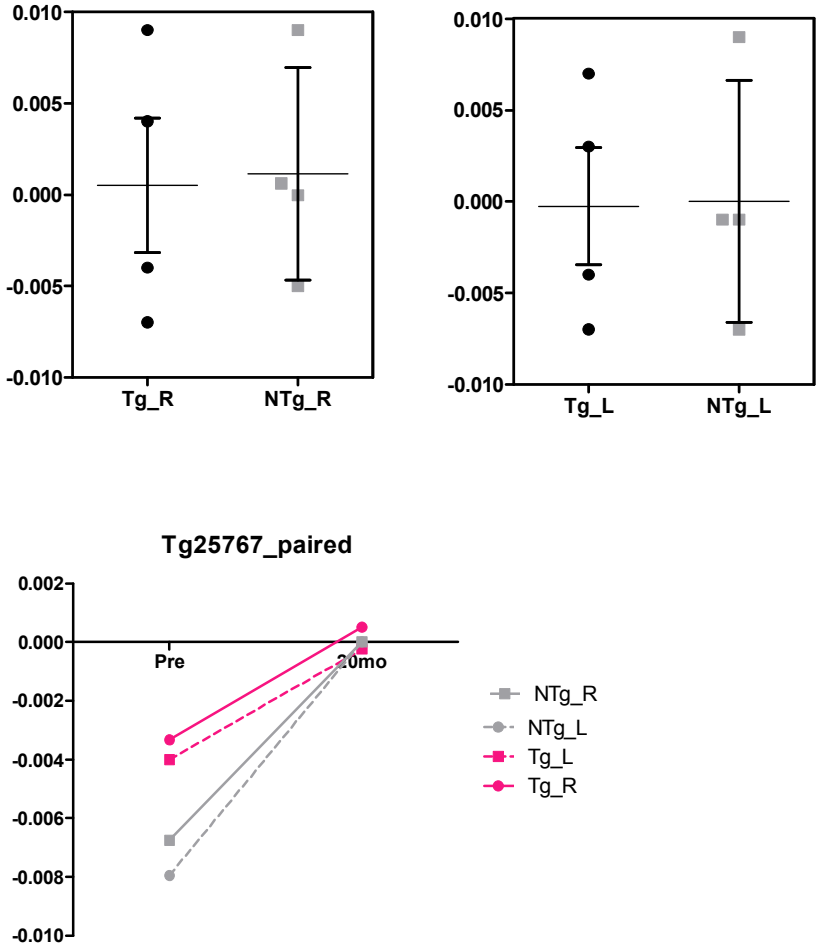

Figure 10. Scatter dot plots of CBV, CBF, Leakage parameters and temporal change of permeability index in Tg2576

For ROI analyses of clusters obtained from VBM result showed significant differences in left hippocampus and subiculum. Raw data is shown in Table 6.

	Lt hippocampus	Lt subiculum
Tg1	-6.53E-03	-1.56E-02
Tg2	-4.40E-03	-1.49E-02
Tg3	-5.99E-02	6.37E-04
Tg4	-1.31E-03	-9.48E-04
NTg1	-3.25E-02	-3.43E-02
NTg2	-4.22E-02	-5.78E-02
NTg3	-3.92E-02	-4.42E-02
NTg4	-2.50E-02	-3.89E-02
Cluster size	38	38
p-value	0.0286	0.0286

Table 6. Values of leakage obtained from two different areas from Tg2576 (Tg) and age-matched non-transgenic (NTg) mice.

Extracted values from two clusters, left hippocampus and subiculum, were analyzed.

III.1.3. Histology findings in Alzheimer transgenic mice

I evaluated the amyloid beta (Aβ) plaque and pericyte in frontal cortex and dorsal hippocampus of 5xFAD mice with 8 months old. I found diffused, large amounts of Aβ deposition (Figure 11) in transgenic mice while few positive cells existed in control mice. As for pericyte, there seemed an higher numbers of $PDGF\beta^{+}$ cells were in transgenic group

comparing to control group (Figure 12). PDGFβ^{+} cells in 5xFAD mice were characterized by hypertrophic, disorganized morphology.

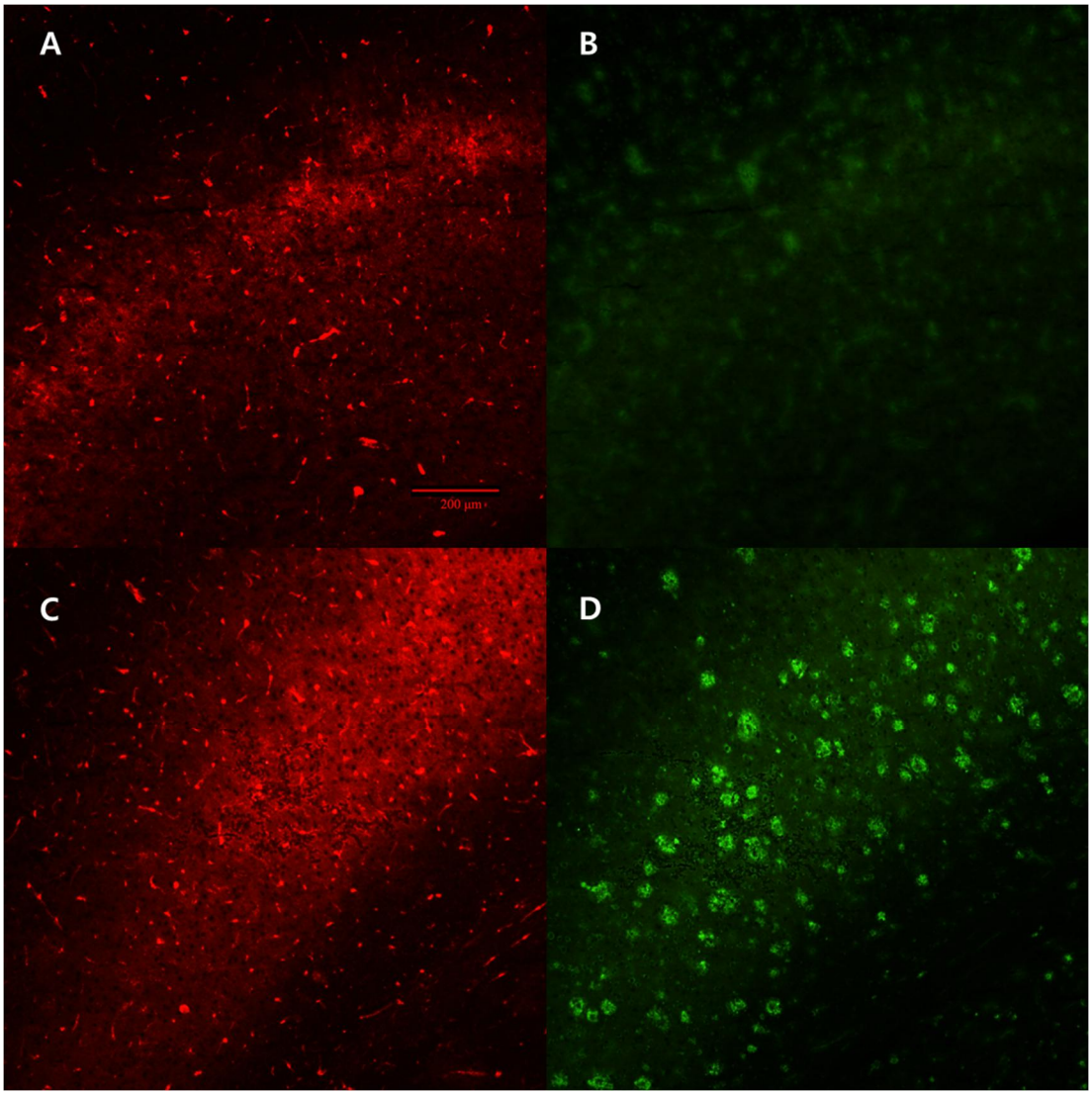

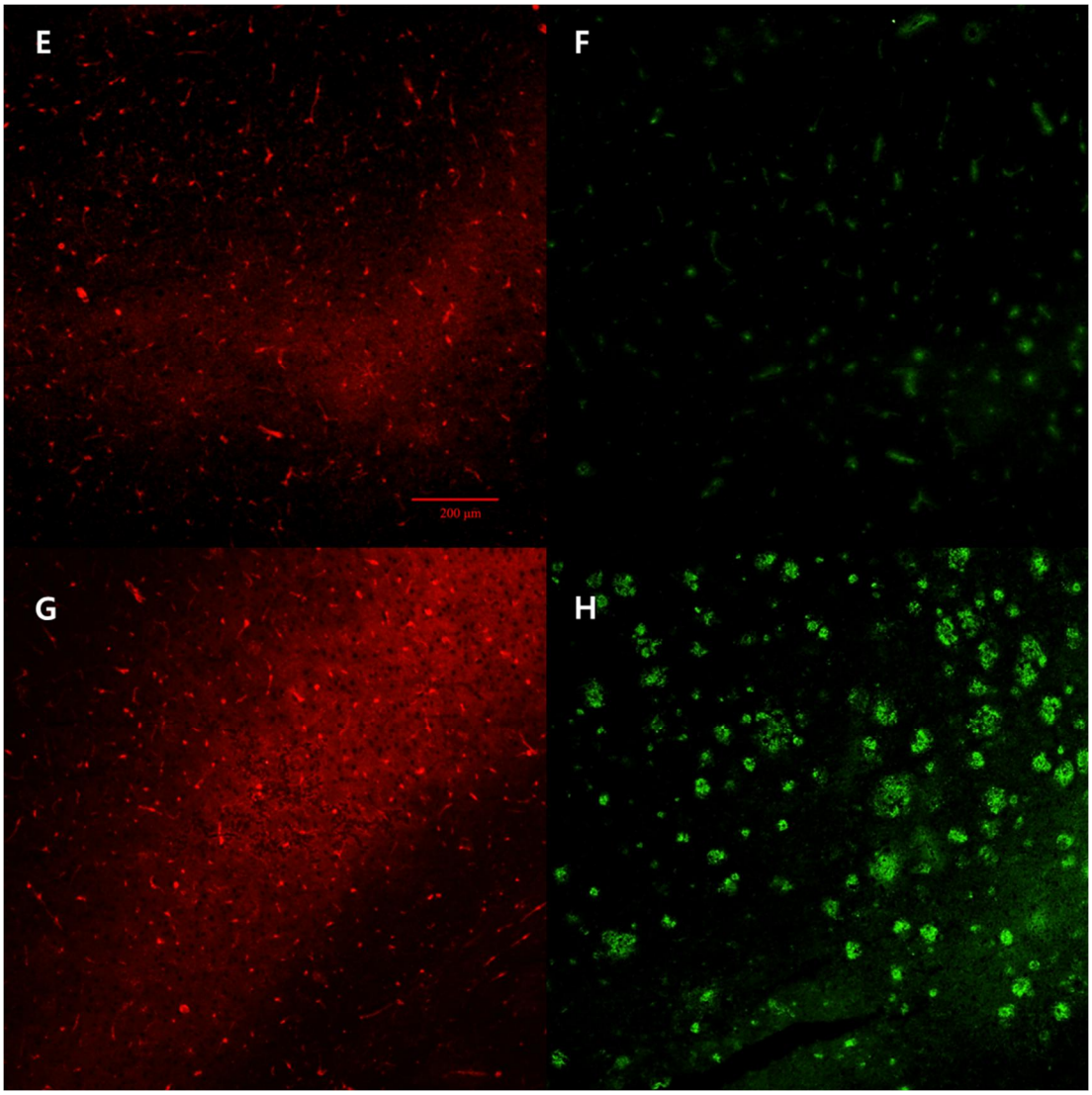

Figure 11. Immunohistologic findings in 5xFAD mice compared with controls

A-D, left frontal cortex; E-H, right dorsal hippocampus. Amyloid plaque deposition is remarkable in frontal cortex and dorsal hippocampus of 5xFAD transgenice mice.(D,H) Pericytes in transgenic mice seems hypertrophic and disorganized (C,G) compared with the controls (A,E)

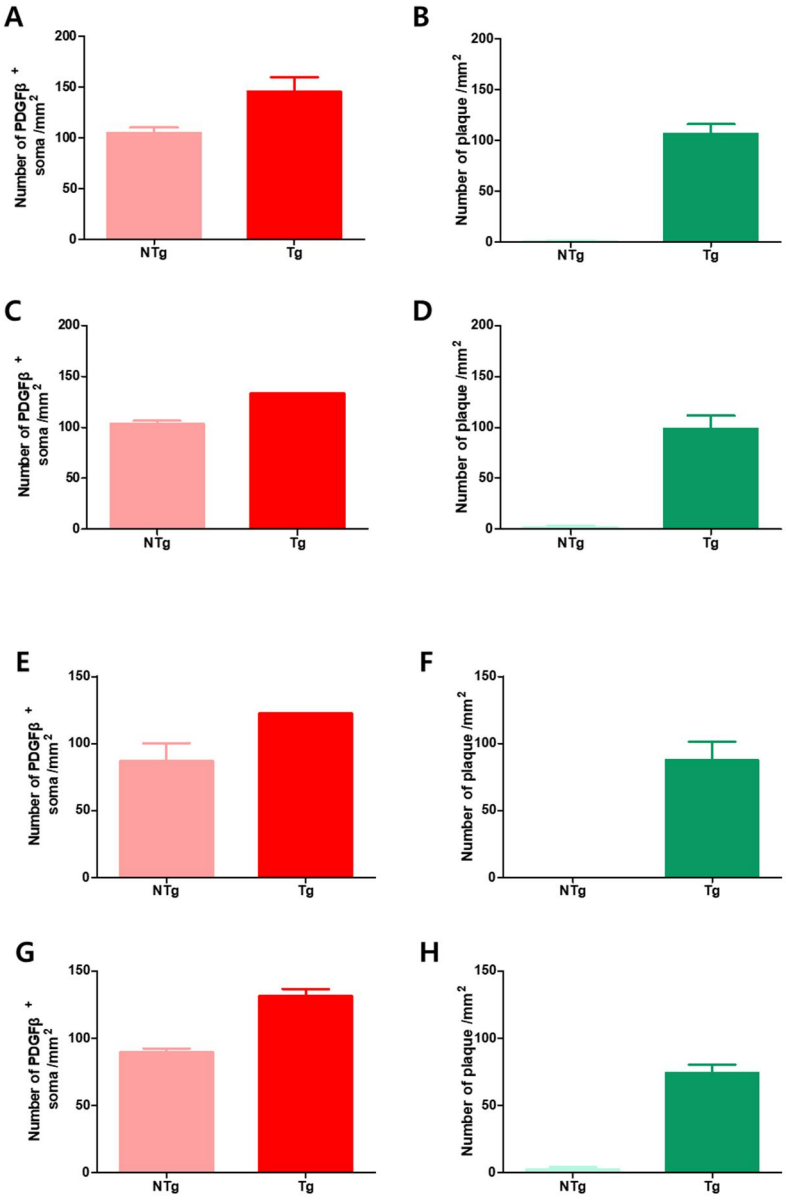

Figure 12. Number of pericytes and amyloid plaques in 5xFAD mice compared with non-transgenic mice

A-D, frontal cortex; E-H, dorsal hippocampus. (A,B,E,F) left. (C,D,G,H) right.

III.2. Human study

III.2.1.Voxel Based Analysis

a) Group comparison

The DSC-MRI in a subset of 10 participants (mean age 68.1±10.9 years) with clinical AD was compared with those in 13 normal controls (mean age 69.9±7.0 years). Figure 13 shows the results comparing perfusion indices between two groups. Analyses of regional leakage indices indicated that BBB permeability was higher in AD patients, particularly in right putamen (p=0.012) and thalamus (p=0.035). I also analyzed the extraction fraction maps, CBV, CBF, and MTT maps. AD group showed higher values in left corpus callosum ($p<$ 0.001), right cingulate gyrus (p= 0.004) and parahippocampal gyrus (p= 0.016) in extraction fraction map. CBF, CBV and MTT parameters were also calculated and analyzed. AD patients showed higher values CBF, CBV maps whereas no significant difference existed on MTT map (Figure 13, Table 7). In GM and WM analysis both parameters showed higher values in normal controls than in AD patients (Figure 14).

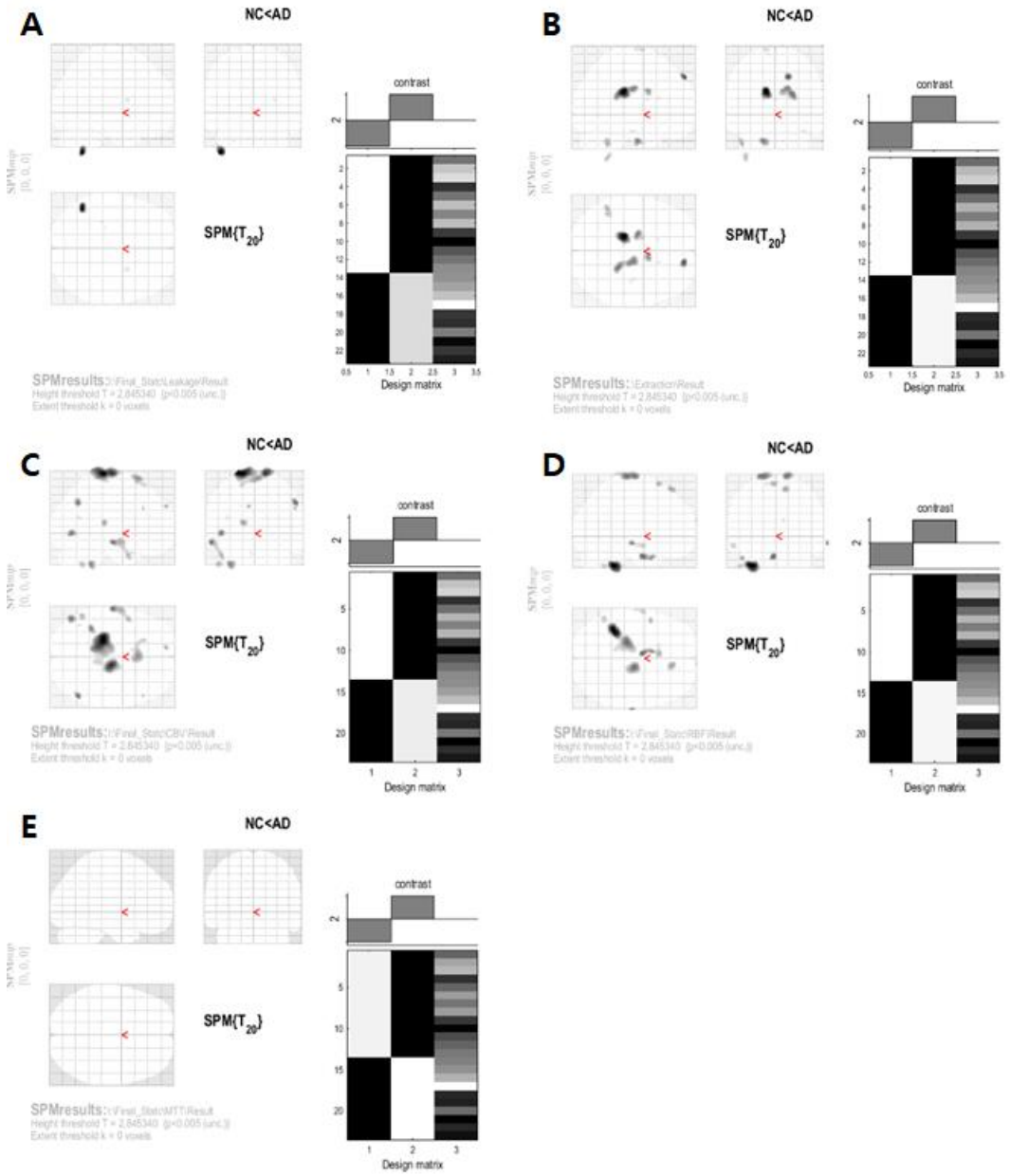

Figure 13. VBM analysis of leakage parameters in human

A, Region of higher leakage index in AD group; **B**, Region of higher extraction fraction index in AD group; **C**, Region of higher CBV index in AD group; **D**, Region of higher CBF index in AD group; **E**, Region of higher MTT index in AD group.

	vox_x	vox_y	vox_z	cluster size	z-score
Leakage map					
	-46	-58	-50	92	3.58
	*2	-10	8	91	3.53
	*28	4	14	21	2.69
Extraction fraction					
	*-14	-30	26	256	3.54
	*16	54	44	34	3.22
	*22	-38	22	224	3.05
	*-18	-10	-34	78	3.05
	*10	4	26	69	2.93
	-48	-52	-36	38	2.85
	-42	-52	-54	34	2.78
	*-14	-4	76	32	2.70
	*38	-18	-22	6	2.61
CBV					
	-20	-28	78	1280	3.52
	54	-64	38	46	3.11
	-62	-16	-14	206	3.07
	-48	-72	-2	78	3.04
	-36	-46	-42	81	3.01
	2	20	70	202	2.93
	-18	-28	12	41	2.90
	-10	58	34	13	2.85
	-52	-58	-42	32	2.78
CBF					
	-36	-44	-42	334	3.50
	-4	-4	-30	84	3.09
	-18	-26	78	322	3.09
	14	-16	78	184	3.07
	70	-20	-12	13	3.02
	12	36	60	51	2.88
	-48	8	-32	22	2.84
	-4	18	68	47	2.83
	-50	-58	-42	29	2.72
	-60	-2	-16	43	2.71

Table 7. VBM analysis of leakage parameters in human

Coordinate xyz, cluster size and z-core of significant area ($p < 0.005$) of perfusion indices. vox, voxel

*, ROI analyses were done

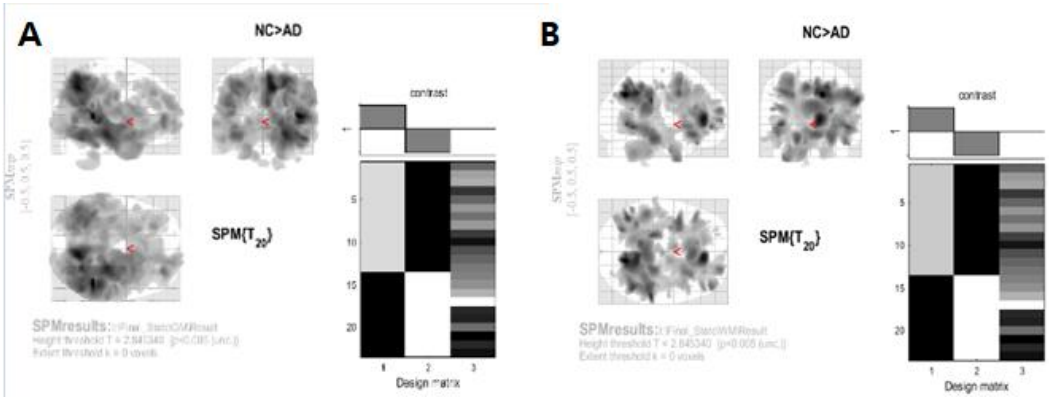

Figure 14. VBM analysis of brain tissue in human

A, Region of higher volume of GM in normal group; **B**, Region of higher volume of WM in normal group.

b) Correlation analyses

We also analyzed whether the permeability indices were correlated with MMSE score. As shown in Figure 15, low MMSE score was correlated with higher extraction fraction index in age-adjusted regression analysis. CBV, CBF, and MTT maps also showed correlation with low MMSE score while no region of correlation existed on a leakage map (Table 8). For brain tissue, GM and WM volume was correlated with higher MMSE score (Figure 16).

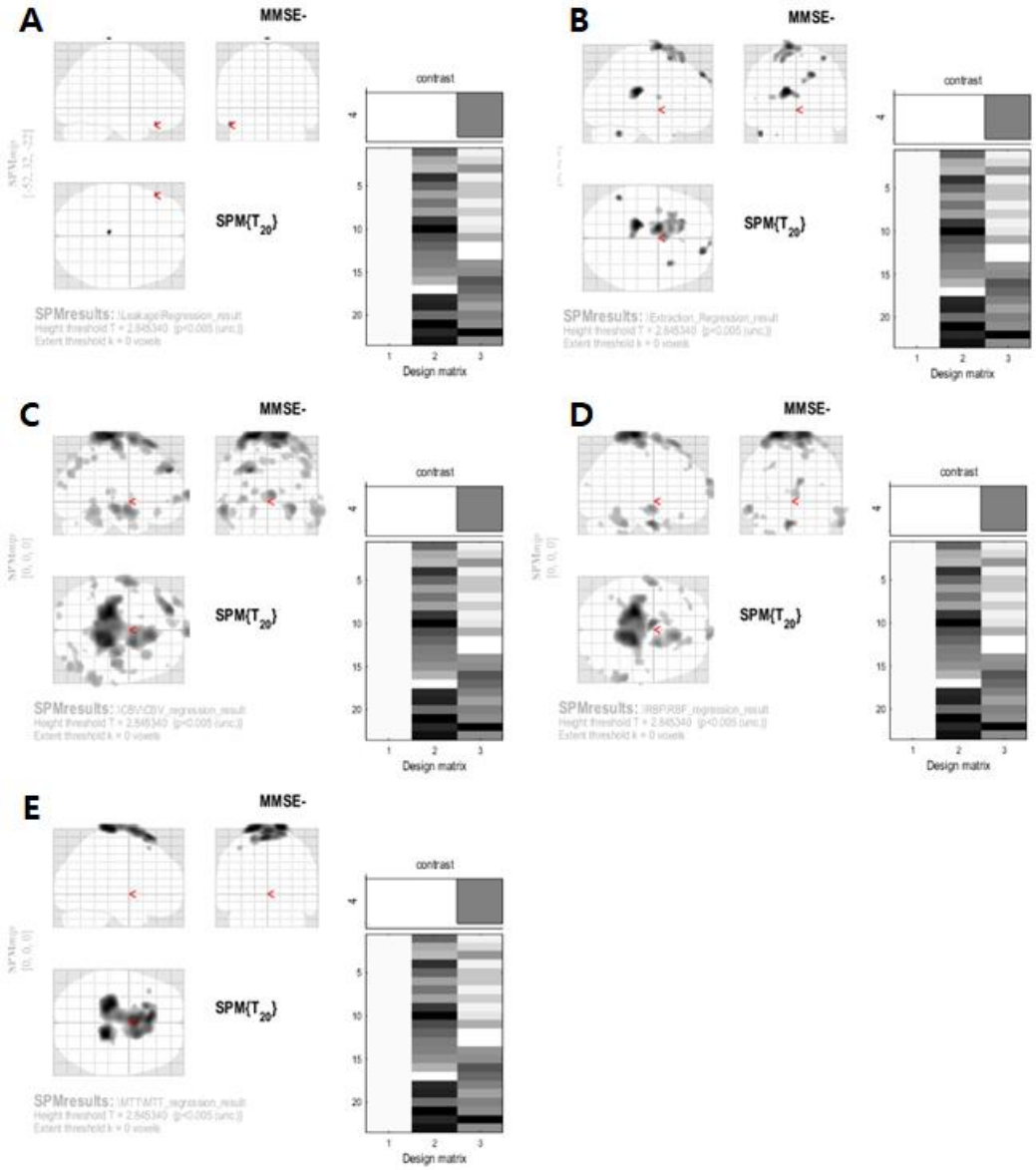

Figure 15. Correlation analysis of MMSE score and perfusion indices in human

Low MMSE score was correlated with extraction fraction, CBV, CBF, and MTT maps. **A**, Region of higher leakage index in AD group; **B**, Region of higher extraction fraction index in AD group; **C**, Region of higher CBV index in AD group; **D**, Region of higher CBF index in AD group; **E**, Region of higher MTT index in AD group.

	vox_x	vox_y	vox_z	cluster size	z-score
Extraction fraction					
	-16	-30	20	323	3.43
	-10	-2	78	853	3.32
	18	56	44	94	3.19
	-50	-54	-32	38	3.14
	34	14	64	38	3.05
	-34	-2	14	34	2.78
CBV					
	-20	-28	80	5954	4.52
	-24	52	38	531	3.96
	32	-18	-12	426	3.61
	-60	-4	-14	594	3.60
	4	76	6	224	3.55
	-34	62	2	133	3.21
	64	-48	-16	627	3.21
	48	-66	50	428	3.11
	-54	-48	54	54	3.04
	-18	-30	10	46	2.98
	38	-88	16	26	2.92
	-30	-94	20	36	2.92
	-48	36	-16	78	2.91
	-20	-14	-12	95	2.90
	4	-58	48	54	2.88
	-8	54	50	83	2.87
	-62	-50	0	36	2.83
	-16	-94	36	26	2.81
	56	2	-34	38	2.81
CBF					
	-20	-26	82	3644	4.21
	-6	-2	-32	265	3.60
	10	28	70	717	3.44
	-58	-4	-12	220	3.27
	8	72	22	227	3.27
	64	-40	-30	407	3.17
	-8	16	66	99	2.85
	-28	46	44	49	2.85
	-34	-48	-42	66	2.81
	-48	34	-22	32	2.81
MTT					
	-22	-26	80	3180	3.41

Table 8. Correlation analysis of perfusion indices in human

Coordinate xyz, cluster size and z-core of significant area ($p < 0.005$) of perfusion indices. vox, voxel

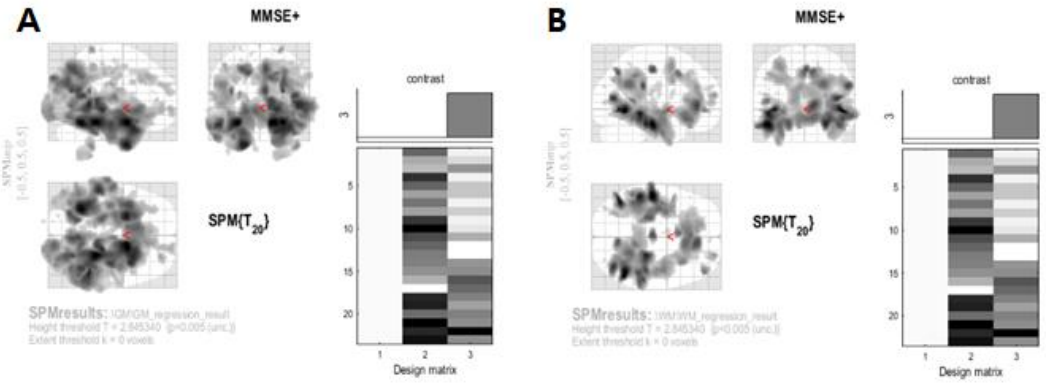

Figure 16. Correlation analysis of MMSE score and brain tissue in human

A, Region of higher volume of GM in higher MMSE score; **B**, Region of higher volume of WM in higher score.

III.2.2. ROI Analysis

I compared the values of right and left hippocampus, precuneus and thalamus obtained from atlas-based ROI. None of the region showed significant difference between two groups, while raw values of the region from VBM analyses showed significant differences between AD patients and controls (Table 9). There was no higher region in controls than AD patients.

	Leakage		Extraction		
	Putamen, Rt	**Thalamus, Rt**	**corpus callosum, Lt**	**cingulate gyrus, Rt**	**parahippocampal gyrus, Rt**
AD 1	1.68E-01	2.05E-01	7.76E+00	9.92E+00	8.66E+00
AD 2	1.83E-02	8.63E-02	2.67E+00	3.68E+00	4.05E+00
AD 3	2.84E-03	5.37E-02	4.56E+00	4.55E+00	2.45E+00
AD 4	1.46E-02	1.18E-01	5.34E+00	2.35E+00	9.40E+00
AD 5	1.07E-01	5.30E-02	7.46E+00	3.99E+00	7.47E+00
AD 6	1.40E-01	2.36E-01	8.75E+00	8.18E+00	7.09E+00
AD 7	9.79E-02	1.79E-01	8.37E+00	8.95E+00	6.50E+00
AD 8	6.54E-02	2.63E-01	6.75E+00	4.30E+00	3.53E+00
AD 9	6.23E-02	2.10E-01	6.94E+00	6.81E+00	2.86E+00
AD 10	6.76E-02	2.16E-01	6.16E+00	5.39E+00	4.00E+00
NC 1	3.52E-02	1.06E-01	4.86E+00	4.79E+00	5.01E+00
NC 2	5.85E-02	1.30E-01	6.36E+00	4.08E+00	3.37E+00
NC 3	1.31E-02	9.63E-02	5.20E+00	2.57E+00	5.53E+00
NC 4	2.34E-02	1.91E-01	3.32E+00	4.38E+00	6.93E+00
NC 5	3.46E-02	1.41E-01	2.96E+00	3.63E+00	3.06E+00
NC 6	1.40E-02	3.94E-02	3.53E+00	3.21E+00	3.71E+00
NC 7	5.37E-03	3.18E-02	2.40E+00	4.00E+00	2.51E+00
NC 8	1.99E-02	1.14E-01	3.09E+00	2.36E+00	1.98E+00
NC 9	3.27E-02	6.14E-02	2.38E+00	2.57E+00	2.44E+00
NC 10	5.14E-02	1.28E-01	4.13E+00	3.37E+00	3.69E+00
NC 11	1.31E-02	8.76E-02	4.71E+00	3.60E+00	1.67E+00
NC 12	1.66E-02	1.00E-01	2.91E+00	2.09E+00	1.74E+00
NC 13	6.92E-02	1.33E-01	4.06E+00	3.98E+00	1.72E+00
***p* value**	1.20E-02	3.50E-02	0.0005	0.0043	0.0162
Age adjustment	N	Y	Y	Y	Y

Table 9. Raw data of human DSC-MRI parameters (Leakage, Extraction fraction)

IV. Discussion

In this study, a novel approach extracting leakage parameters from DSC-MRI was applied to mice and human brain to assess regional BBB permeability in AD. In preclinical study with Alzheimer transgenic mice, increasing tendency of permeability indices existed between transgenic and control group. Furthermore, temporal change of permeability with increasing age was noticeable in transgenic group. Human data also revealed higher permeability indices in severe regions of AD patients with DSC-MRI.

IV.1. BBB permeability in AD model and AD patients

IV.1.1. Animal study

Various studies historically investigated BBB dysfunction in AD patients, postmortem samples, or in mouse models and these led to heterogeneous results. Early studies via DCE-MRI showed no difference between AD patients or age-matched controls.[35] There was also a molecular study showing that that wide spread BBB leakage is lacked in aged Alzheimer transgenic mice.[36] Recently, there is developing evidence indicating that BBB breakdown

occurs in normal aging or early in demented patients.[3 23 37-40] Our study showed no significant difference in ROI-analysis of hippocampus between transgenic mice and WT mice. This might be explained by small sample size and the timing of MRI scan. Previous study evaluating BBB permeability with DCE perfusion imaging showed increased permeability index in transgenic animals, however in their later stages of the disease (at least 16 months).[20] MRI was performed far earlier in this study, on 4 to 8months of age, which might lead to less clear results allowing for the difference of mouse model. Another considerable factor is that I drew a ROI of whole hippocampus in 10 slices and averaged the values. The degree of leakage might have been underestimated considering that BBB disrupted area is relatively focal on early stage as shown in our voxel based analysis. When I compared the values obtained from voxel based analysis, there showed clear difference between two groups. While most preclinical studies have been conducted cross-sectional study including two or more age groups, I designed the study as a follow up study with 4 month-interval to observe the change of permeability index and minimize the inter-subject variations. For serial follow-up of MRI in 5xFAD, the change of

permeability indices were prominent in transgenic mice, which indicates the accelerated leakage extent in a disease model.

IV.1.2. Human study

Previous studies of AD patients have shown that BBB disruption begins at early stage of the disease, though the initial region is still controversial. Early BBB breakdown appeared in the hippocampus and its CA1 and dentate gyrus subregions in individuals with MCI[23] while in early stage of AD several gray and white matter regions were found to be leaky.[11 14] Recent study of DCE-MRI showed that BBB breakdown in AD appeared to be widespread rather than focal.[24] Our findings revealed higher permeability in several GM and WM regions of AD patients, but not in hippocampus. Negative results of atlas-based ROI data would be explained by same reason of mice data as mentioned above; As the leakage is focal and heterogeneous even in hippocampus, mean values of whole hippocampus might underestimate results. In multiple regression analysis with age and MMSE score, old age and low MMSE score showed correlation with increased permeability however the clusters were not enough to adjust for

multiple comparisons. MMSE scores and disease duration, which represent the severity of the disease, were also heterogeneous in AD group, which might have been a confounding factor. Further study with large size and amyloid proven cohort is needed for statistical significance.

IV.2. Pericyte dysfunction in 5xFAD mice

The BBB-associated mural cells, in particular pericyte plays a key role in the formation and maintenance of the BBB. Pericyte degeneration has been shown to lead to BBB disruption at capillary levels and several immunohistological and electron microscopy studies showed that degeneration and loss of brain capillary pericyte in AD and AD models.[41-43] Our data seems paradoxical as PDGFRβ^+ cells rather increased in transgenic group more than in control group while the amount of amyloid plaque was obvious in the former. A possible explanation for these results may be related to the age of mice. Recent study of 5xFAD mice showed that during degradation of pericyte, from 9 to 12 months age, there was an transient increase in number of PDGFRβ^+ soma, characterized by hypertrophic or disorganized ramifications.[44]

Hypertrophic PDGFRβ^{+} pericyte processes were also found in Tg2576 mic with late-stage of AD, resulting in and increased, disorganized perivascular coverage.[45)]

IV.3. DSC-MRI

I used DSC-MRI to evaluate the vascular permeability in this study. Conventionally DSC-MRI has been used for CBF and CBV measurements, while DCE-MRI for permeability measurements. DCE-MRI is used mostly as a research tool rather than clinical use, because of the long examination time. Whereas, DSC-MRI has relatively short scan time (~ 5 minutes) which is more suitable for demented patients. With understanding of underlying physics, DSC-MRI was recently suggested for estimating vascular permeability in tumor.[31)] Implementation of common DSC-MRI leakage-correction techniques afforded the elicitation of rate constants postulated to report on vessel permeability. In this study, I showed that age-dependent leakage rate differed in Alzheimer transgenic mice from controls with serial follow up DSC-MRI. This is noteworthy in a regard that studies displaying trends in same mice with perfusion imaging is sparse. I also showed increasing tendency of permeability index at earlier age in transgenic

mice than previously reported.[20 36] Our results support previous findings of vascular contributions to AD and suggest DSC-MRI as a suitable tool for estimating BBB breakdown in AD.

IV.4. Limitations

Limited by number of participants, correlation with age or cognitive profile of the subject was not analyzed in present study. Furthermore, amyloid beta status was not evaluated with PET or CSF study, which raised the uncertainity of the diagnosis in AD group. However, I've screened patients in memory clinic of neurology department with full sequence MRI and neuropsychological test, then enrolled the patients with clinical diagnosis of AD. I also excluded the participants with other risk factors causing dementia including depression, stroke, hypertension and diabetes mellitus.

V. Conclusion

This is the first study applying DSC-MRI to AD patients to assess BBB disruption. I suggest DSC-MRI as a feasible imaging biomarker for vascular permeability measurements in neurodegenerative disease through further evaluation with extended disease spectrum and large cohort.

References

1. Jiang Q, Ewing JR, Chopp M. MRI of blood-brain barrier permeability in cerebral ischemia. *Translational stroke research* 2012;3(1):56-64. doi: 10.1007/s12975-011-0133- [published Online First: 2012/03/01]
2. Erickson MA, Banks WA. Blood-brain barrier dysfunction as a cause and consequence of Alzheimer's disease. *J Cereb Blood Flow Metab* 2013;33(10):1500-13. doi: 10.1038/jcbfm.2013.135 [published Online First: 2013/08/08]
3. Chakraborty A, de Wit NM, van der Flier WM, et al. The blood brain barrier in Alzheimer's disease. *Vascular pharmacology* 2017;89:12-18. doi: 10.1016/j.vph.2016.11.008 [published Online First: 2016/11/30]
4. Zlokovic BV. Neurovascular pathways to neurodegeneration in Alzheimer's disease and other disorders. *Nature reviews Neuroscience* 2011;12(12):723-38. doi: 10.1038/nrn3114 [published Online First: 2011/11/04]
5. Nicolakakis N, Hamel E. Neurovascular function in Alzheimer's disease patients and experimental models. *J Cereb Blood Flow Metab* 2011;31(6):1354-70. doi: 10.1038/jcbfm.2011.43 [published Online First: 2011/04/07]
6. Fiala M, Liu QN, Sayre J, et al. Cyclooxygenase-2-positive macrophages infiltrate the Alzheimer's disease brain and damage the blood-brain barrier. *European journal of clinical investigation* 2002;32(5):360-71. [published Online First: 2002/05/25]
7. Zipser BD, Johanson CE, Gonzalez L, et al. Microvascular injury and blood-brain barrier leakage in Alzheimer's disease. *Neurobiol Aging* 2007;28(7):977-86. doi: 10.1016/j.neurobiolaging.2006.05.016 [published Online First: 2006/06/20]
8. Ryu JK, McLarnon JG. A leaky blood-brain barrier, fibrinogen infiltration and microglial reactivity in inflamed Alzheimer's disease brain. *Journal of cellular and molecular medicine* 2009;13(9a):2911-25. doi: 10.1111/j.1582-4934.2008.00434.x [published Online First: 2008/07/29]
9. Hultman K, Strickland S, Norris EH. The APOE varepsilon4/varepsilon4 genotype potentiates vascular fibrin(ogen) deposition in amyloid-laden vessels in the brains

of Alzheimer's disease patients. *J Cereb Blood Flow Metab* 2013;33(8):1251-8. doi: 10.1038/jcbfm.2013.76 [published Online First: 2013/05/09]

10. Goos JD, Kester MI, Barkhof F, et al. Patients with Alzheimer disease with multiple microbleeds: relation with cerebrospinal fluid biomarkers and cognition. *Stroke* 2009;40(11):3455-60. doi: 10.1161/strokeaha.109.558197 [published Online First: 2009/09/19]
11. van de Haar HJ, Jansen JFA, Jeukens C, et al. Subtle blood-brain barrier leakage rate and spatial extent: Considerations for dynamic contrast-enhanced MRI. *Medical physics* 2017;44(8):4112-25. doi: 10.1002/mp.12328 [published Online First: 2017/05/12]
12. Xu G, Bayly PV, Taber LA. Residual stress in the adult mouse brain. *Biomechanics and modeling in mechanobiology* 2009;8(4):253-62. doi: 10.1007/s10237-008-0131-4 [published Online First: 2008/07/25]
13. Nation DA, Sweeney MD, Montagne A, et al. Blood-brain barrier breakdown is an early biomarker of human cognitive dysfunction. *Nat Med* 2019;25(2):270-76. doi: 10.1038/s41591-018-0297-y [published Online First: 2019/01/16]
14. van de Haar HJ, Jansen JFA, van Osch MJP, et al. Neurovascular unit impairment in early Alzheimer's disease measured with magnetic resonance imaging. *Neurobiol Aging* 2016;45:190-96. doi: 10.1016/j.neurobiolaging.2016.06.006 [published Online First: 2016/07/28]
15. Law M, Yang S, Babb JS, et al. Comparison of cerebral blood volume and vascular permeability from dynamic susceptibility contrast-enhanced perfusion MR imaging with glioma grade. *AJNR Am J Neuroradiol* 2004;25(5):746-55. [published Online First: 2004/05/14]
16. Faure A, Verret L, Bozon B, et al. Impaired neurogenesis, neuronal loss, and brain functional deficits in the APPxPS1-Ki mouse model of Alzheimer's disease. *Neurobiol Aging* 2011;32(3):407-18. doi: 10.1016/j.neurobiolaging.2009.03.009 [published Online First: 2009/04/29]
17. Poisnel G, Herard AS, El Tannir El Tayara N, et al. Increased regional cerebral glucose uptake in an APP/PS1 model of Alzheimer's disease. *Neurobiol Aging*

2012;33(9):1995-2005. doi: 10.1016/j.neurobiolaging.2011.09.026 [published Online First: 2011/11/15]

18. Hebert F, Grand'maison M, Ho MK, et al. Cortical atrophy and hypoperfusion in a transgenic mouse model of Alzheimer's disease. *Neurobiol Aging* 2013;34(6):1644-52. doi: 10.1016/j.neurobiolaging.2012.11.022 [published Online First: 2013/01/01]
19. Kassner A, Roberts T, Taylor K, et al. Prediction of hemorrhage in acute ischemic stroke using permeability MR imaging. *AJNR Am J Neuroradiol* 2005;26(9):2213-7. [published Online First: 2005/10/13]
20. Chiquita S, Ribeiro M, Castelhano J, et al. A longitudinal multimodal in vivo molecular imaging study of the 3xTg-AD mouse model shows progressive early hippocampal and taurine loss. *Human molecular genetics* 2019 doi: 10.1093/hmg/ddz045 [published Online First: 2019/03/01]
21. Caserta MT, Caccioppo D, Lapin GD, et al. Blood-brain barrier integrity in Alzheimer's disease patients and elderly control subjects. *The Journal of neuropsychiatry and clinical neurosciences* 1998;10(1):78-84. doi: 10.1176/jnp.10.1.78 [published Online First: 1998/04/21]
22. Starr JM, Farrall AJ, Armitage P, et al. Blood-brain barrier permeability in Alzheimer's disease: a case-control MRI study. *Psychiatry research* 2009;171(3):232-41. doi: 10.1016/j.pscychresns.2008.04.003 [published Online First: 2009/02/13]
23. Montagne A, Barnes SR, Sweeney MD, et al. Blood-brain barrier breakdown in the aging human hippocampus. *Neuron* 2015;85(2):296-302. doi: 10.1016/j.neuron.2014.12.032 [published Online First: 2015/01/23]
24. van de Haar HJ, Burgmans S, Jansen JF, et al. Blood-Brain Barrier Leakage in Patients with Early Alzheimer Disease. *Radiology* 2017;282(2):615. doi: 10.1148/radiol.2017164043 [published Online First: 2017/01/19]
25. Simultaneous blood volume and permeability mapping using a single Gd-based contrast agent. Proceedings of the Annual Meeting of the International Society for Magnetic Resonance in Medicine; 1994 August 6–12; San Francisco, California.
26. Sorensen AG, Wray SH, Weisskoff RM, et al. Functional MR of brain activity and perfusion in patients with chronic cortical stroke. *AJNR Am J Neuroradiol*

1995;16(9):1753-62. [published Online First: 1995/10/01]

27. Boxerman JL, Schmainda KM, Weisskoff RM. Relative cerebral blood volume maps corrected for contrast agent extravasation significantly correlate with glioma tumor grade, whereas uncorrected maps do not. *AJNR Am J Neuroradiol* 2006;27(4):859-67. [published Online First: 2006/04/14]
28. Lee B, Park JE, Bjornerud A, et al. Clinical Value of Vascular Permeability Estimates Using Dynamic Susceptibility Contrast MRI: Improved Diagnostic Performance in Distinguishing Hypervascular Primary CNS Lymphoma from Glioblastoma. *AJNR Am J Neuroradiol* 2018;39(8):1415-22. doi: 10.3174/ajnr.A5732 [published Online First: 2018/07/22]
29. Lee JY, Bjornerud A, Park JE, et al. Permeability measurement using dynamic susceptibility contrast magnetic resonance imaging enhances differential diagnosis of primary central nervous system lymphoma from glioblastoma. *Eur Radiol* 2019 doi: 10.1007/s00330-019-06097-9 [published Online First: 2019/03/17]
30. Ahn K-C, Learman CR, Dunbar GL, et al. Characterization of Impaired Cerebrovascular Structure in APP/PS1 Mouse Brains. *Neuroscience* 2018 doi: https://doi.org/10.1016/j.neuroscience.2018.05.002
31. Skinner JT, Moots PL, Ayers GD, et al. On the Use of DSC-MRI for Measuring Vascular Permeability. *AJNR Am J Neuroradiol* 2016;37(1):80-7. doi: 10.3174/ajnr.A4478 [published Online First: 2015/10/03]
32. Mouridsen K, Friston K, Hjort N, et al. Bayesian estimation of cerebral perfusion using a physiological model of microvasculature. *NeuroImage* 2006;33(2):570-9. doi: 10.1016/j.neuroimage.2006.06.015 [published Online First: 2006/09/15]
33. Mouridsen K, Hansen MB, Ostergaard L, et al. Reliable estimation of capillary transit time distributions using DSC-MRI. *J Cereb Blood Flow Metab* 2014;34(9):1511-21. doi: 10.1038/jcbfm.2014.111 [published Online First: 2014/06/19]
34. Coupe P, Yger P, Prima S, et al. An optimized blockwise nonlocal means denoising filter for 3-D magnetic resonance images. *IEEE transactions on medical imaging* 2008;27(4):425-41. doi: 10.1109/tmi.2007.906087 [published Online First: 2008/04/09]

35. Schlageter NL, Carson RE, Rapoport SI. Examination of blood-brain barrier permeability in dementia of the Alzheimer type with [68Ga]EDTA and positron emission tomography. *J Cereb Blood Flow Metab* 1987;7(1):1-8. doi: 10.1038/jcbfm.1987.1 [published Online First: 1987/02/01]

36. Bien-Ly N, Boswell CA, Jeet S, et al. Lack of Widespread BBB Disruption in Alzheimer's Disease Models: Focus on Therapeutic Antibodies. *Neuron* 2015;88(2):289-97. doi: 10.1016/j.neuron.2015.09.036 [published Online First: 2015/10/24]

37. Sweeney MD, Montagne A, Sagare AP, et al. Vascular dysfunction-The disregarded partner of Alzheimer's disease. *Alzheimer's & dementia : the journal of the Alzheimer's Association* 2019;15(1):158-67. doi: 10.1016/j.jalz.2018.07.222 [published Online First: 2019/01/16]

38. Raja R, Rosenberg GA, Caprihan A. MRI measurements of Blood-Brain Barrier function in dementia: A review of recent studies. *Neuropharmacology* 2018;134(Pt B):259-71. doi: 10.1016/j.neuropharm.2017.10.034 [published Online First: 2017/11/07]

39. Ku MC, Waiczies S, Niendorf T, et al. Assessment of Blood Brain Barrier Leakage with Gadolinium-Enhanced MRI. *Methods in molecular biology (Clifton, NJ)* 2018;1718:395-408. doi: 10.1007/978-1-4939-7531-0_23 [published Online First: 2018/01/18]

40. Montagne A, Zhao Z, Zlokovic BV. Alzheimer's disease: A matter of blood-brain barrier dysfunction? *J Exp Med* 2017;214(11):3151-69. doi: 10.1084/jem.20171406

41. Sweeney MD, Ayyadurai S, Zlokovic BV. Pericytes of the neurovascular unit: key functions and signaling pathways. *Nature neuroscience* 2016;19(6):771-83. doi: 10.1038/nn.4288 [published Online First: 2016/05/27]

42. Sagare AP, Bell RD, Zhao Z, et al. Pericyte loss influences Alzheimer-like neurodegeneration in mice. *Nature communications* 2013;4:2932. doi: 10.1038/ncomms3932 [published Online First: 2013/12/18]

43. Park L, Zhou P, Koizumi K, et al. Brain and circulating levels of Abeta1-40 differentially contribute to vasomotor dysfunction in the mouse brain. *Stroke* 2013;44(1):198-204. doi: 10.1161/strokeaha.112.670976 [published Online First: 2012/12/04]

44. Giannoni P, Arango-Lievano M, Neves ID, et al. Cerebrovascular pathology during the

progression of experimental Alzheimer's disease. *Neurobiology of disease* 2016;88:107-17. doi: 10.1016/j.nbd.2016.01.001 [published Online First: 2016/01/17]

45. Park L, Zhou J, Zhou P, et al. Innate immunity receptor CD36 promotes cerebral amyloid angiopathy. *Proceedings of the National Academy of Sciences of the United States of America* 2013;110(8):3089-94. doi: 10.1073/pnas.1300021110 [published Online First: 2013/02/06]

Abstract (Korean)

Dynamic Susceptibility Contrast Magnetic Resonance Imaging (DSC-MRI)을 이용한 알츠하이머 치매에서 혈관 투과성 평가

연구 배경

알츠하이머 치매는 아밀로이드 단백과 타우 단백의 이상 침착을 특징으로 하는 퇴행성 뇌질환이다. 그러나 최근 혈관성 인자도 알츠하이머 치매의 병태생리에서 중요한 역할을 한다고 보고되며, 특히 뇌혈관 장벽의 역할이 중요할 것으로 보고 있다. 치매와 같은 퇴행성 뇌질환에서 일어나는 미세한 뇌혈관 장벽의 손상을 영상으로 보는 것은 쉽지 않지만, 최근 몇 연구에서 perfusion MRI를 통해 이를 보였다. 그 중에서도 Dynamic susceptibility contrast (DSC) MRI는 짧은 시간 안에 뇌혈관 장벽의 손상을 보여주는 새로운 영상기법으로서 가능성이 있다. 그러나 이제까지 알츠하이머 치매에서 혈관 투과성을 보는 데에 DSC-MRI를 적용해본 연구는 없었다. 따라서, 우리는 동물 실험과 임상 데이터를 통해 DSC-MRI의 임상적용 가능성을 보이고자 한다.

연구 방법

동물 실험을 위해 5xFAD 와 Tg2576 두가지 종류의 알츠하이머 모델 쥐를 사용하였으며 연령대가 같은 정상군 쥐와 함께 하였다. 결과적으로 총 13마리의 5xFAD 와 8마리의 Tg2576 쥐에서 T1, T2, 가돌리늄 조영제 주입 후 DSC-MRI를 분석하였다. Cerebral blood volume (CBV), cerebral blood flow (CBF), extraction fraction, leakage 영상을 얻었고 이를 Region of Interest (ROI) 와 voxel-based analysis 로 분석하였다. MRI 이후에는 쥐의 뇌를 채취하여 염색 후 병리소견을 보았다. 임상에서는 23명 (10명의 알츠하이머 치매 환자와 13명의 정상군)의 DSC-MRI를 분석하였다.

연구 결과

5xFAD 쥐에서 정상군에 비해 해마에서 뇌혈관 장벽의 손상이 증가하는 경향을 보였으며 voxel-based analysis 에서는 left frontal cortex 와 dorsal hippocampus에서 통계적으로 의미 있는 차이를 보였다. 시간에 따른 뇌혈관 장벽의 손상도는 치매군 쥐에서 뚜렷한 증가를 보였다. 임상 데이터 분석 결과, right

putamen과 thalamus에서 leakage map의 유의미한 차이가 있었고, left corpus callosum 과 right cingulate gyrus, parahippocampal gyrus에서 extraction fraction map의 차이를 보였다.

결론

DSC-MRI를 통해 알츠하이머 치매 모델 쥐에서 뇌혈관 장벽의 손상이 정상군에 비해 심한 것을 확인하였다. 알츠하이머 치매 환자에서도 뇌의 회색질과 백색질 영역 일부에서 정상군과 차이를 보였다. 따라서, DSC-MRI는 알츠하이머 치매 환자에서 뇌혈관 장벽의 손상을 평가하는 imaging biomarker 로서의 가능성을 보였으며 추가적인 큰 규모의 임상시험을 통해 이를 증명해갈 수 있을 것이다.